ISSN: 0067-2904

Investigating a Filtered Feedback Weight in the Output Signal to Simulate a Self-learning Layer in an Optical Neural Network

Dhuha Raad Madhloom[1]*, Ayser A. Hemed[2], Suha Mousa Khorshed[1]
[1] *Department of Physics, College of Science, Al-Nahrain University, Baghdad. Iraq*
[2] *Department of Physics, College of Education, Mustansiriyah University, Baghdad. Iraq*

Received:18 /11 /2023 Accepted: 20 /10/2024 Published: 15 /2/2025

Abstract

An edge-emitting semiconductor laser (SL) source with a wavelength of 1310 nm is used experimentally to follow a transmitted signal that is subject to selected modifications. SL maximum measured optical power was -11 dBm at a temperature of 24ºC, which is configured as a chaotic influencer semiconductor laser (ISL) in a unit of an optical neural network. The weight of the sent signal, after division, is controlled by two uniform Fiber Bragg gratings (FBGs) with slightly different periods. In addition, the feedback strength is changed by two radio frequency attenuators. The passing signal via these two filters is detected and summed again before being directly modulated and re-injected to the ISL again via the bias current. The results confirm a variable chaotic FWHM and bandwidth as a function of applied parameters. Emission for selected strengths is controlled by radio frequency attenuators after the power division. For each opto-electronic feedback (OEFB) branch, a noticeable difference in Fourier space is noted in addition to time and phase spaces.

Results indicate a large variation in the calculated number of spikes (4268 to 71330) and also in the calculated FWHM (0.80991-10.5928) MHz This indicates the possibility of deriving the SL in a different number of quantum states by introducing filtered chaotic dynamics. Generalizations for the effect of optical weights, achieved in this study, open the door to increasing the processing speed in the processing units of computers and self-learning terms in robots.

Keywords: Chaotic Modulation, Optoelectronic Feedback, Fiber Bragg Grating, Deep Learning, and Semiconductor Laser.

استقصاء ثقل التغذية الراجعة المفلترة على الاشارة الخارجة لمحاكاة طبقة التعلم الذاتي في شبكة عصبية بصرية

ضحى رعد مظلوم*[1]، أيسر عبدالحسين حمد[2]، سهى موسى خورشيد[1]
[1]قسم الفيزياء، كلية العلوم، جامعة النهرين، بغداد–العراق
[2]قسم الفيزياء، كلية التربية، الجامعة المستنصرية، بغداد–العراق

الخلاصة

تم استخدام مصدر ليزر شبة موصل ذو الانبعاث الجانبي وطول موجي 1310 نانومتر لمتابعة إشارة

*Email: duha.raad23@gmail.com

مرسلة معرضة لتعديلات مختارة. القدرة الضوئية المقاسة عمليا لليزر بلغت −11ديسي بيل عند درجة حرارة 24 درجة مئوية حيث استخدم الليزر كمؤثر فوضوي يحاكي وحدة شبكة عصبية ذات طبيعة ضوئية. تم التحكم بثقل الإشارة المرسلة بعد شطرها ضوئيا بواسطة اثنين من المرشحات نوع فايبر براغ بينهما اختلاف محدد في قيمة الترشيح. يتم تغيير قدرة الجزئين الناتجين من الإشارة الاصلية بواسطة اثنين من موهنات التردد اللاسلكي. تم الكشف عن الاشارة النافذة من كل من هذين المرشحين بواسطة كاشف ضوئي لكل خط من الشطرين وعرضهما على الاوسلسكوب قبل إعادة جمعهما وإعادة تحميلهما على مدخل الليزر. وجد تفاوت ملحوظ في طبيعة الديناميكية الفوضوية المرصودة عند كل شطر والتي كانت دالة للمتغير المفروض. حصل تزايد اسي في عدد القمم المتولد اثر كل قياس وبشكل متزايد يتراوح بين القيمتين (4268 to 71330). باحصاء كامل الاستعراض عند منتصف الشدة للطيف الترددي المقاس وجد تزايد مشابه في القيم المقاسة بحيث كانت القيم تتراوح ضمن الفترة الترددية: (0.80991−10.5928) MHz.

النتيجة اكدت عمليا ان الانبعاث الفوضوي الذي ولدة الليزر تحت هذه الظروف كان قابلا للتحكم ومتغايرا في الشطر الأول عنه في الشطر الثاني. تشير النتائج الى انتقال متسارع من مستوي كمي معين في المادة الفعالة لليزر الى مستوي اخر منتجا ديناميكية مختلفة في كل مره واشارة مرصودة بعد الشطر أيضا مختلفة. هذا يدل على وجود ترددات جديدة تتولد داخل التجويف الذاتي لليزر بفعل تأثر معلمات المادة الفعالة لا خطيا. ان تأثر شكل الخرج الليزري يمثل تطويرا لسلوكه وتعميمه يعتبر تطبيقا ناجحاً في وحدة المعالجة للحواسيب الشخصية وللتعلم الذاتي في الروبوتات.

1. Introduction

The idea of Artificial Neural Networks (ANNs) was developed after a based model on algebra with algorithms was developed in 1943 by A. McCulloch and W. Pitts [1]. Thompson described and simulated the mechanisms and principles of the living cells of the nerve [2]. In 1957, Frank Rosenblatt, a psychologist, designed the perceptron algorithm and reported it in a major publication [3]. Applying that method, Rosenblatt developed the first single-layered perceptron, shown in Figure (1), an electrical computing device that fits in the biological theories underlying human brain (HB) function.

Conductance-based neuronal types are a class of modular and physiologically real computer simulations for individual neurons built using the Hodgkin-Huxley architecture [3]. The nonlinear dynamics of these systems connect the passage of ion currents in and out of a neuron to the time evolution of its membrane voltage. They reflect the continuous-valued potential at the membrane versus the binary-valued collection of spike events and so can cause a wide variety of neuronal actions, including bursts, spikes of various waveforms, and threshold oscillations [4].

The structure, functions, and use of energy of the human brain are a great source of inspiration. Neuromorphic computing and neuromorphic engineering refer to this broad idea of creating neural systems and applying complex neuron models to replicate the internal workings of the brain [5].

These different neuron models act on the same basic idea: at a threshold input signal, neurons receive multiple synapses' input signals that are added together, and a corresponding output is fired. Machine Learning (ML), a subset of Deep Learning (DL), is composed of Artificial Intelligence (AI). The living brain's deep architecture, which consists of billions of linked neurons acting as processing units, is a model that is very similar to learning work. Similar to how our brains work, models for DL divide up incoming data into features, then merge them back together to finish tasks (e.g., detection, classification), and can be used to perform similar tasks automatically once they have learned key characteristics during the training phase [6].

Goodman et al. at Stanford college first proposed the theoretical concept of an optical vector-matrix multiplier in 1978 [7]. This developed into a significant advancement in optical computing that aided in the study of Optical Matrix Multiplication (OMM) and the creation of photonic neural networks [8].

The aim of the current study is to prove the effectiveness of optical signal filtering and attenuating in resulted dynamics after summing them. This effect depends on the existence of OEFB to stimulate nonlinear dynamics of SL, which is considered an optical self-learning in this unit of an optical neural network.

FBGs serve as optical filters because they have a stop band or frequency range where most incident light is reflected back; they are employed in sensor applications and as a narrow band transmission or reflection filter. All wavelengths, except those equal to Bragg wavelength (λ_B), are unaffected by FBG and travel through the FBG transmission side [9]. Remaining wavelengths are totally reflected from FBG slits, which is named deflected light, and directed to the reflection side. The apodization method can represent these side branches [10]. Modes and reversed modes interaction based on coupled equations starting with the nonlinear Schrödinger equation for a signal propagating inside the optical fiber can be used to determine the spectral profile of a pulse passing within a typical (one region) Bragg grating [11]:

$$\frac{\partial u^{+}}{\partial z} - i\left[k - \frac{1}{2}(\Delta\beta - \frac{\partial\varphi(z)}{\partial z}\right]u^{+}exp^{-i[\Delta\beta-\emptyset(z)]} = 0 \quad (1)$$

$$\frac{\partial u^{-}}{\partial z} + i\left[k - \frac{1}{2}(\Delta\beta - \frac{\partial\varphi(z)}{\partial z}\right]u^{-}exp^{i[\Delta\beta-\emptyset(z)]} = 0 \quad (2)$$

Where: k is the coupling coefficient between outgoing (u^{+}) and incoming (u^{-}) modes flowing within FBG region, $\Delta\beta$ is the mismatching in the signals phase, which is given as: $\Delta\beta = (w - w_B).\frac{n_{eff}}{C}$, such that n_{eff} is the effective index for core, C is the speed of light at Bragg wavelength λ_B given by Filho and Chaves [12], $\lambda_B = 2n_{eff}\Lambda$, calibrating with this parameter, Bragg frequency $w_B = \frac{\pi C}{n_{eff}\Lambda}$, can be determined and $\emptyset$ is the grid period chirp that vanishes for the uniform FBG.

2. Theoretical concepts

To create a more abstract high-level model for characteristic categories or elements by constructing a neural network, DL entails learning the rules, representing levels for sample data and gathering low-level features. The three elements, information, formulas, and power for computation, are crucial for the development of DL methods and technologies [13]. It may mimic how the HB works during analytical learning to find distributed feature representations for data, enabling it to use basic models to do hard learning tasks like classification [14]. The tools supporting DL have been available for decades, and in the last few years, with the accessibility of many datasets with advancements in technological devices, they have undergone constant change. Excellent algorithms are now a key component of AI technological advances, like neural networks used for DL [15]. Neuromorphic systems try to translate artificial intelligence and machine learning algorithms onto massively distributed hardware that can physically simulate the human brain for computational and simulation needs. Applications of neuromorphic systems have already been thoroughly investigated in the technology field, leading to the development and improvement of breakthroughs like field-effect transistors and memristors. More attention has recently been paid to optical neuromorphic systems for alternatives due to the importance of its Von Neumann shortage, the inherent challenges of electrical wiring, and the exponential development of chip power [13].

Optical neuronal networks and photonics circuits offer a revolutionary specialized neural network accelerator technique for using parametric changes in optics for computation. Systems for optical computing can be parallel or massively integrated with tiny form factor devices. Compared to electronics, photonics has the benefits of broad bandwidth, rapid speed, and low power consumption. Photonic technologies may greatly decrease the electrical power consumption of data and logic processes. Chaotic operations with photons may be implemented directly using a wide range of intrinsic optical nonlinearities. After training, a neural network can have a passive design and execute calculations on its optical signal without requiring extra energy input [16].

One property for Generating Chaos (GC) is increased transmission capacity in secure optical communications. Using direct modulation into SLs (uploading modulation onto erratic carriers themselves) can result in chaos.

Chaotic instability in laser intensity may arise when an external pump modulation is introduced for a laser system, altering the pumping current. It is necessary to equalize the external modulation of frequency surrounding the laser to prevent the nonlinear reaction between that frequency and a subsequent frequency from creating GC. The method used to include the frequency component loss modulation, often known as External Frequency Modulation (EFM), is the disappearance of the internal laser cavity. However, the quasi-periodicity pathway to chaos, which is inversely proportional to the intensity of EFM, is often used to investigate chaotic processes. In the last ten years, innovative sensors, such as optical fibers and fiber sensors, have advanced quickly. Single-mode fibers with a broad bandwidth and low loss are attracting a lot of attention in the field of optical communication [17].

The link between sensors and optical communications has been introduced recently, especially for dynamic security systems based on GC. The choice is the selective filtered feedback approach, which uses a quarter-wavelength shift and single-distributed feedback to make the lasers in the laser cavity oscillate at the Bragg wavelength λ_B [18].

The relaxation oscillation frequency (f_{RO}) can convey the damped oscillatory movement by doing a linear stability analysis on the laser rate formulae with respect to the intrinsic laser and operational parameters. They are then expressed as [19], [20]:

$$f_{RO} = \frac{1}{2\pi}\sqrt{\frac{\xi I_s}{\tau_p}} \tag{3}$$

Where: I_s is the steady-state intensity, ξ is the gain coefficient, and τ_p is the photon lifetime. Keep in mind that ξ depends on the operational parameters, particularly the bias current. They get damped at a rate provided by [19]:

$$\Gamma_{RO} = \frac{1}{\tau_c} + \xi I_s \tag{4}$$

Where τ_c is the carrier lifetime.

Unwanted reflections are stopped using optical isolators. The filtered optical feedback (OFB) laser can be represented by rate equations for the lasers' complex-valued optical field

(E), real-valued population inversion (N), and complex-valued optic field (F) of the filter. These formulas can be expressed as dimensionless forms, which are [21]:

$$\frac{dE}{dt} = (1 + i\alpha)N(t)E(t) + kF(t) \quad (5)$$

$$T\frac{dN}{dt} = P - N(t) - \big(1 + 2N(t)\big)|E(t)|^2 \quad (6)$$

$$\frac{dF}{dt} = \Lambda E(t - \tau)e^{-iC_p} + (i\Delta - \Lambda)F(t) \quad (7)$$

Where: α is the line-width amplification factor, k is the OFB rate, T is the electron lifetime, P is the pump rate, which determines the material properties of the laser, C_p is the feedback phase, τ is the delay time that arises from the finite propagation time of the light in the external feedback loop, Δ is the detuning between the filter center frequency and solitary laser frequency, and Λ is the filter width represented by a line-shape function.

The coupling term between laser and filter in Equation (3) is kF(t). Complex envelope F in Equation (5) of the filter field is derived by assuming a single Lorentzian approximation for the Fabry–Perot filter. There are other possibilities related to filtered OFB, such as that reported by Ghayib and Hemed [22]. A positive optoelectronic technique for chaotic generation and diagnosis through statistics for both the number of spikes and line shape for signals is an effective tool in this field [23]. Dhyaa et al. [24] investigated and approved signal weight after demultiplex was applied. One of these two demultiplexed signals was subjected to selected phase change relative to the other. The follower SL obeyed chaotic responses with high sensitivity to phase variation.

Partial optical filtering followed with optoelectronic feedback to the SL device itself is also approved experimentally by Hemed and Ghayib [25], to which stimulate SL chaotic emission was achieved.

Relaxation oscillations are the source of excluding dimensions. They result from a regular energy exchange between the laser's population inversion (the number of electron-hole pairs) and the optical field (the number of photons). Their characteristic frequency, which is in the range of GHz, depends on the laser and its working parameters.

As an essential application for the current study, Figure (1) illustrates how the summation of the limit or the biophysical interactions varies from one another by weight W_N. The neuron models covered here are vital to a neural-network model known as neural networks spiking, given that they aid in simulating the biological processes of the brain [1].

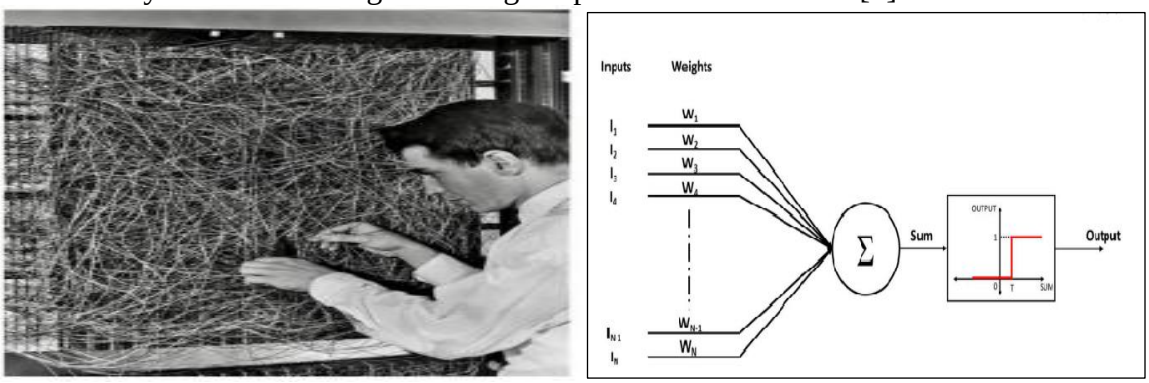

(A) (B)

Figure 1 : Neuron artificial simulation and model (without learning term). (A) Frank Rosenblatt using his single-layer perceptron [26], (B) The McCulloch-Pitts mathematical model to the actual neuron [1].

3. Experimental set-up

The experimental set-up includes an SL source (model HFCT5205A) of a 1310 nm wavelength and a maximum measured optical power of -11 dBm at a temperature of 24^{o}C. The operational wavelength was selected to be compatible with the available equipment in the laboratory, including detectors, FBGs, de-multiplexers, etc. The SL and PDs were supplied with a high-filtered DC power supply to ensure low noise.

As shown in Figure 2(A), the SL signal was split into two measured equivalent parts by an optical fiber splitter (OFS) de-multiplexer(1X2). The two created optical parts passed through separate paths. Both includes: an optical fiber circulator (OFC), with a reflected blocked port, and uniform fiber Bragg gratings (UFBG) (SMF-28E type) with a λ_{B1} of 1310.13 nm, its reflectivity equals 84%. For the second part; λ_{B2} is 1310.36 nm and a reflectivity equals 83%. In addition, two identical photo-detectors (PDs) (model BT-1VE-T) are received those optical signals. Finally, radio frequency attenuators (RF) are used to control signals strengths.

The resulted two output signals are then summed by a fiber multiplexer to mix them with a new form before re-injecting them into the input of SL through OEFB path via direct modulation. The signal after splitting was subjected to two different parameters (RF1 and RF2 attenuators). The results indicated that the responses were different for each part of the signal, which is what we call "weight". In additional to the two Bragg wavelengths, the later parameter represents additional "weights", that can affect the overall signal before re-injecting it to get SL. A mixed-signal oscilloscope (MSO) in each circuit branch observes the signals to evaluate the "weight" of each after the modification. Figure (2A) shows the set-up drawn by the Opti-system program, and a photo of the set-up is shown in Figure (2B).

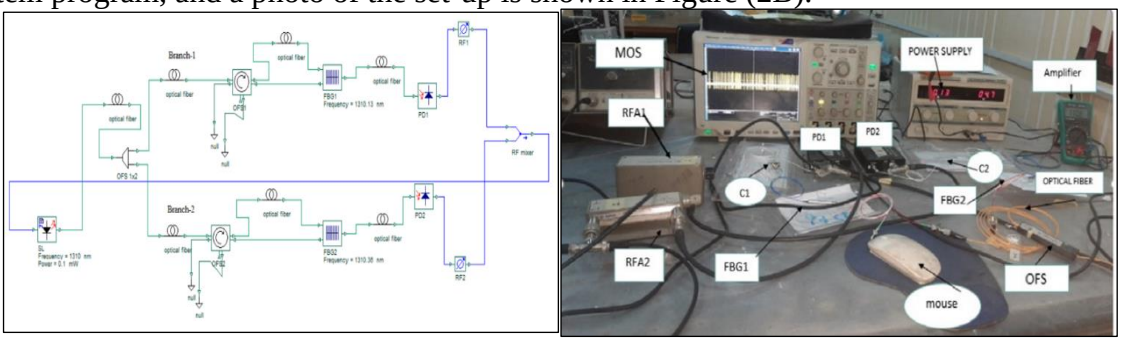

(A) **(B)**

Figure 2: Experimental set-up details. (A) Set-up drawn by Optisystem software for clarity, and (B) Photographic plat for the experimental set-up

4. Results and Discussion

The SL signal undergoes OEFB and filtering by two distinct narrow filters with marginally varying λ_B, according to the setup shown in Figure 1A. This scenario provides a chance to look at the weight of the signal of every feedback branch independently. Through OEFB, the laser reacts to this feedback in a non-linear manner. With this configuration, a simulation was constructed in the laboratory as a calibration to the respond of biological cells. Such simulation is important although a biological system has a communication system based on electrochemical components. Statistics for the signals' FWHM and number of peaks were carried out to diagnose the difference in the signal properties against the applied parameters, which were the laser operation voltage, feedback branch strength, and filtering period. Further measurements for the observed spectra, such as FWHM and the number of peaks were recorded. All the measured parameters by the MSO, such as the optical powers and laser bias current recorded after achieving an accepted signal, are summarized in Table 1. Note that "Rw" in this table (and the coming tables) means "row," which represents a set of measurements including time series, Fast Fourier Transform (FFT), and attractors in the mentioned figures.

Unwanted results, including low signal-to-noise ratios due to different perturbations affecting the laser source, were not measured.

Table 1: Classification details for experimentally measured parameters and its own figures. Att. is attenuation and B-1, B-2 are branch-1 and branch-2 in the optoelectronic circuit, respectively.

ISL Voltage (volt)	ISL current (mA)	RF Att. (dB) (B-2)	RF Att. (dB) (B-1)	Figure No. (B-2) upper Rw.	Figure No. (B-1) lower Rw.
4.9	141.2	10	8	Fig.-4	Fig.-4
4.9	141.1	10	6	Fig.-5	Fig.-5
4.9	141.1	10	4	Fig.-6	Fig.-6
4.9	141.1	10	2	Fig.-7	Fig.-7
4.5	128	2	10	Fig.-8	Fig.-8
4.5	128	4	10	Fig.-9	Fig.-9
4.5	128	6	10	Fig.-10	Fig.-10
4.5	128	8	10	Fig.-11	Fig.-11

During the measurements, the weight of the output signal of each branch of the circuit (Fig. 2A) with the first variable, (RF1) attenuator, was observed while keeping that of branch two at a constant operating value. Table 2 gives another statistic for the laser signals results after multiplexing including the number of peaks, which is equivalent to the number of spikes, and the measured FWHM. The remaining two columns in last table represent the attenuation ratio, which is delivered to the ISL input bias. For all given results, whenever a mismatch existed between the upper and lower rows, the signal weight difference is thus noticeable and considered acceptable. Noting that run no. in this table is divided into two groups: even and odd. Even ones correspond to down rows, while odd ones correspond to upper rows. Then, results, for the sixteen listed run no., are classified to upper including A, B, C referred to by odd listing number in last table, and lower including A, B, C referred to by even listing number in the same table.

Table 2: Statistics details for no. of peaks (spikes), FWHM for Gaussian frequencies, ratio between the ISL's attenuation RFA1/RFA2, and RFA2/RFA1.Odd figure number: upper row, even number: down row.

Run No.	Figure	No. of peak	FWHM (MHz)	RFA1 -RFA2/RFA1	RFA2-RFA1/RFA2
1	5	4268	0.80991	20%	-25%
2	5	450	10.3419	20%	-25%
3	6	12205	13.952	40%	-66.66%
4	6	63881	9.7304	40%	-66.66%
5	7	70629	33.68	60%	-1.5%
6	7	73079	9.8796	60%	-1.5%
7	8	70494	5.6923	80%	400%
8	8	75605	10.28	80%	400%
9	9	70701	8.90598	-400%	80%
10	9	67155	9.6569	-400%	80%
11	10	87665	11.3815	-1.5%	60%
12	10	76222	12.2923	-1.5%	60%
13	11	82463	15.6121	-66.66%	40%
14	11	76466	13.7701	-66.66%	40%
15	12	81910	17.50881	-25%	20%
16	12	71330	10.5928	-25%	20%

From the last table, it is possible to draw a graph representing the overall weight of the attenuation ratio against successive run numbers (Figure 3). In which there exists a relatively low variation between the 20% and 80% in the majority of observations, as shown in Figure 4A, which included all observations except run numbers 9 and 10. For those two observed points, there exist the highest attenuation values that are affecting the smooth resulted curve behavior. In the case of the opposite observation, Figure 4B, the relation is the same, but the two specified points, the same as in Figure 4A, also include irregularities. Hence, these two points represent turning points for the behaviors.

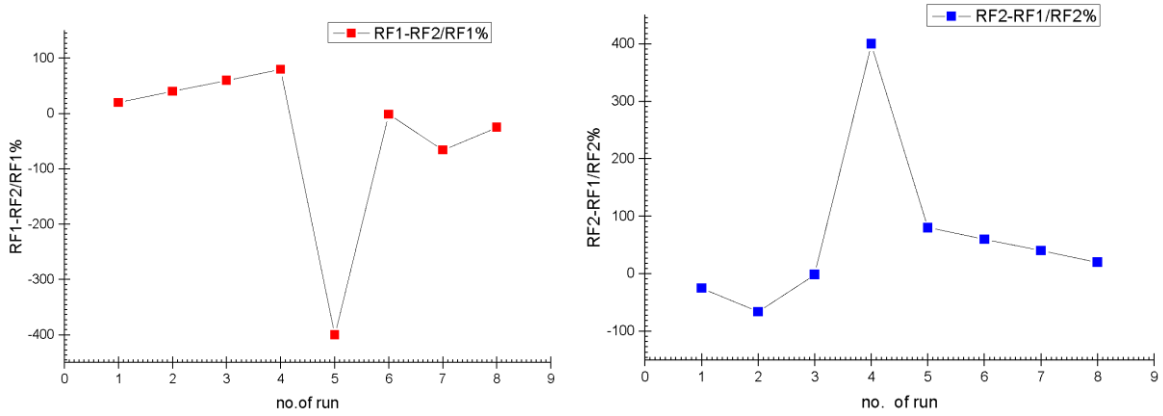

(A) (B)

Figure 3 :Weighted OFB rates prior to (A) filtering and, (B) detection.

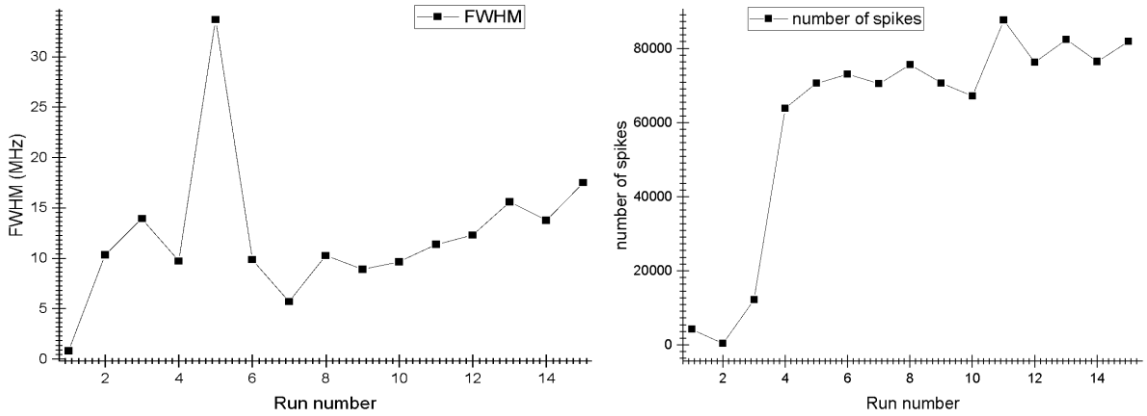

(A) (B)

Figure 4 : Resulted relations for number of runs and obtained parameters for the output signal. (A) Signal FWHM and (B) Number of resulted spikes.

It is concluded from Figure 4B that the number of spikes satisfied an exponential increase curve with an increased number of runs. The characteristic parameter in this observation is the increase in weight of attenuation ratio, i.e., the increase in contrast between feedback strengths for the laser device that produced the number of spikes. The same observation is deduced for Figure 3B, where the FWHM had a huge increase in comparison with the lowest experiment runs.

In Figure 5 both the upper and lower rows show the observed dynamics with the reported parameters. The time series indicates high signal-to-noise ratio. This indicates good signal isolation from external effects and D.C. filtering with power supply. Also, it indicates low ambient temperature for both the laser and photodetector which help in reducing the thermal noise. The calibrated phase space indicated a limit circle with the growth of a second loop, such

that a rout of chaos was generated. The frequency spectrum, seen on the MSO screen, shows a distinguished peak with a relatively large width. Optimization was then introduced to the signal behavior before saving the result. In essence, the signal is unique, dividing it into two parts by a multiplexer offers the possibility for changing the properties of each resulted signal properties.

The upper figures (row 1) in Figure 5 shows that the observed time series has a scale of "µsec" indicating nearly the same entire SL device resonator cavity round trip time. While, the signal amplitude tends to be altered with the variable time scale, i.e., follows chaos spiks characteristics. The frequency spectrum displays full chaotic emission with a 15 MHz bandwidth, whereas this picture become clearer when observe the attractor for the same time series. Fourier space as well gives signal broadening which is broad band spectrum in lower part than that in the upper one. Last space extension confirms increase in signal both bandwidth and subsequently FWHM, i.e., broadened due to the feedback, reaching the value of 8 MHz**.**

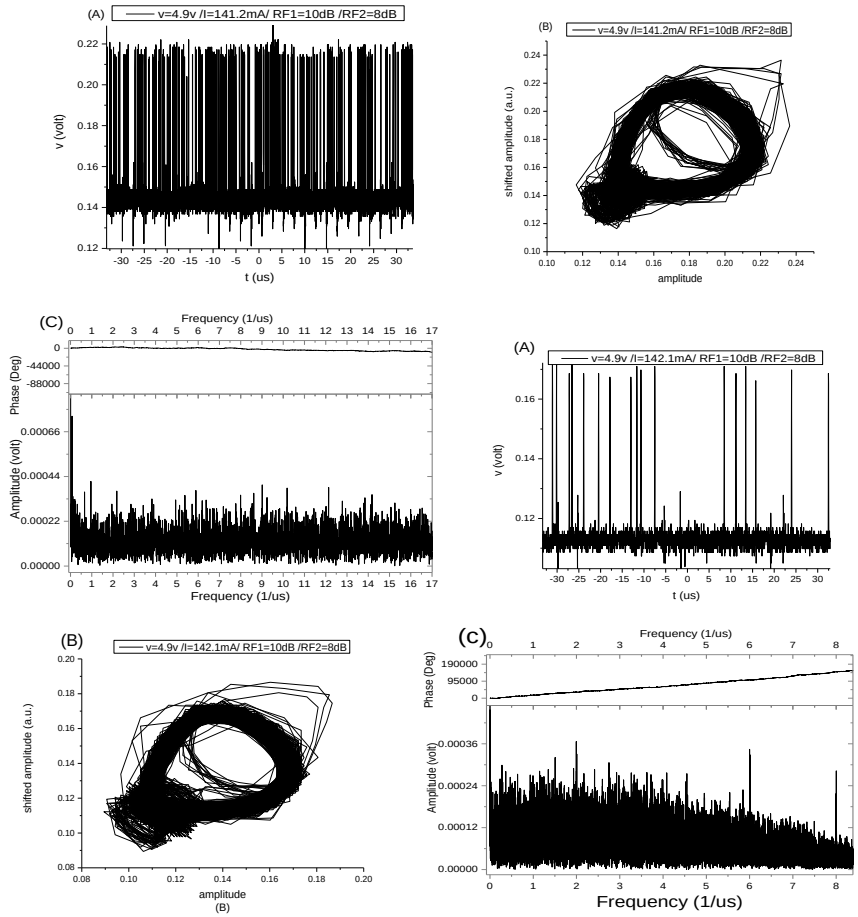

Figure 5 : Results of the experiment using the settings listed in Table 1, run no. 1 with parameters given inside plot. (A) Time series, (B) Calibrated - attractor, and (C) F.F.T.

In Figure 6, row 1, the resulted behavior has evolved to a new state, which is a new stability state. This is within the bifurcation diagram against standard regime for solitary SL device. This transition is under the effect of new dimension provided by the applied feedback. Infinite number of quantum states are presented and can be constructed with such situation. In these initial conditions, the laser is transferred from the previous stability to the present one. The calibrated attractor is changed completely, and the frequency observation is extended further than that observed in the last figure. It is noticed that for the same operational parameters, branch 2 gave a different spectrum, even though both originated from the same laser source.

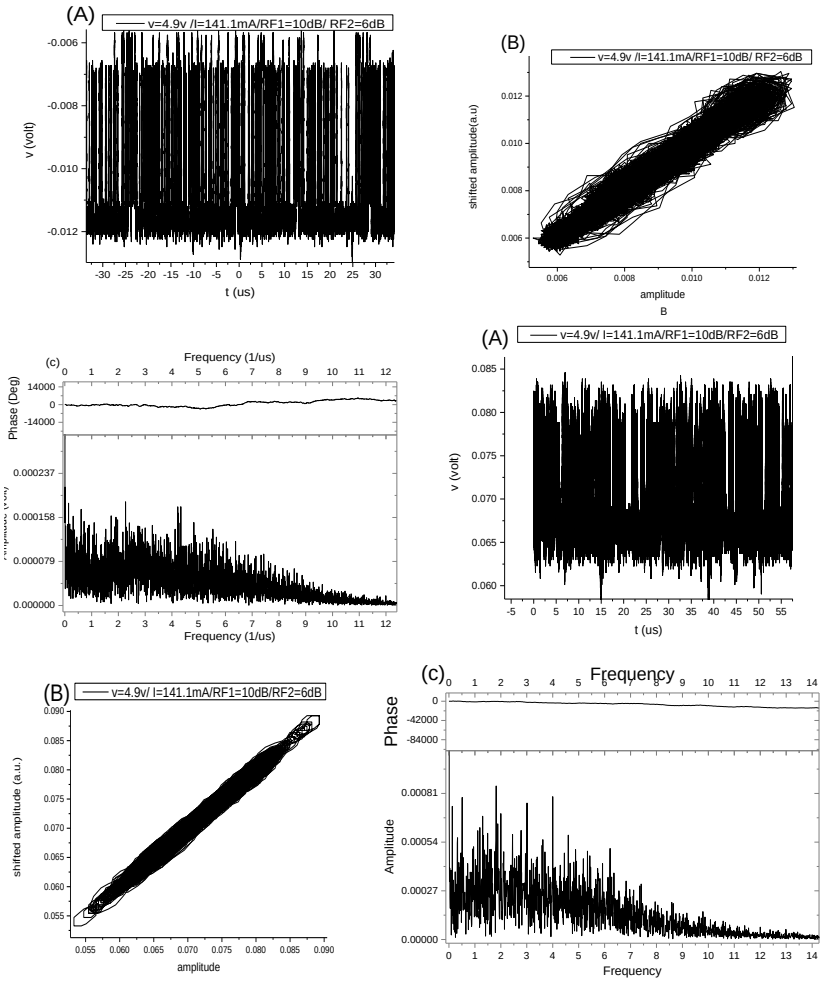

Figure 6 : Experimental results for parameters listed in run no. 2 of Table (1). (A) Time of series, (B) Calibrated-attractor, and (C) F.F.T.

Working in different initial conditions, i.e., changing the attenuation value in branch 2, gave new SL emission characteristics in all spaces, as shown in Figure 7, row 1, including time, calibrated attractor, and frequency space. The SL emission has kept the chaotic specifications but in a different stability state.

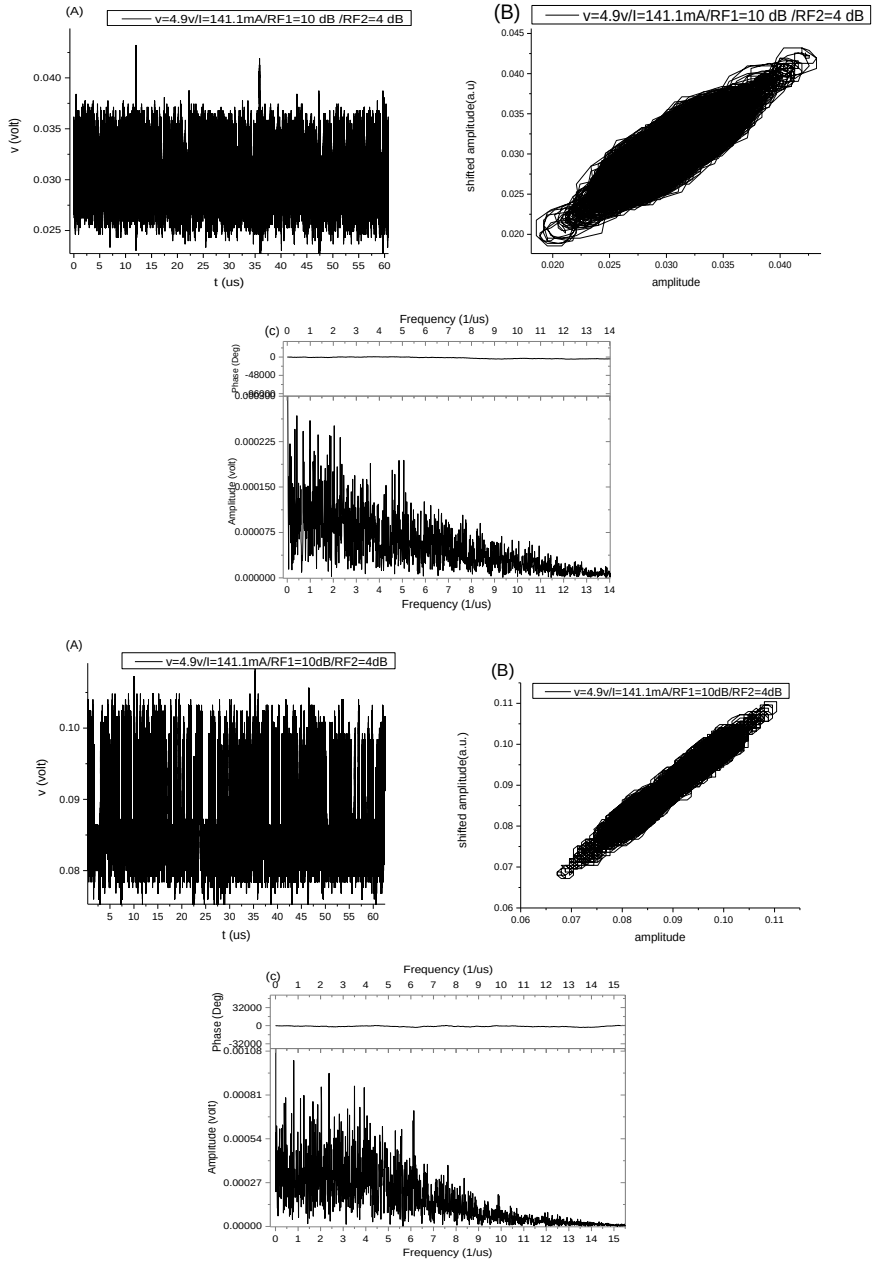

Figure 7 : Experimental results for the parameters listed Table.1 in run no.3 and parameters given inside plot. (A) Time of series, (B) Calibrated attractor, and (C) F.F.T.

Reducing attenuation, i.e., increasing the feedback strength (Figure 8), the transformed SL emission in both branches within the bifurcation area. This means it is possible to send two separate signals with different transmitting codes to separate terminals. This situation simulates a biological order in which a message needs to be sent from one source to different terminals with different codes.

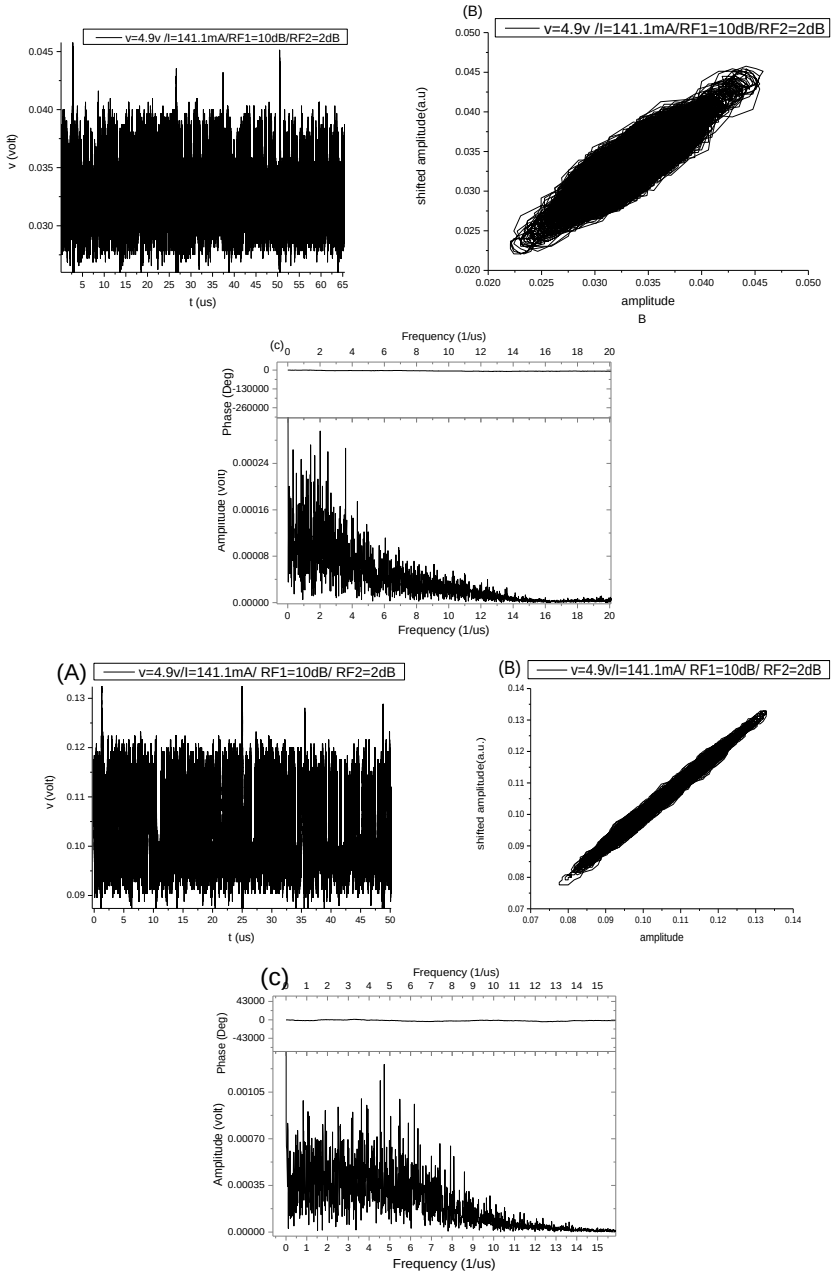

Figure 8 : Experimental results for parameters listed in run no. 4. (A) Time of series, (C) Calibrated attractor, and (C) F.F.T.

A decrease of the SL bias, Figure 9, made its emission more chaotic, with different time durations between each of the two consecutive peaks. This reflects the essential behavior of chaotic dynamics. There was an observed height peak with nearly constant amplitude in the time series, equivalent to the broadened Gaussian pulse seen in the frequency space, such as the results produced from the technique of optical injection in cases of low injected power, as reported by Mercier [20].

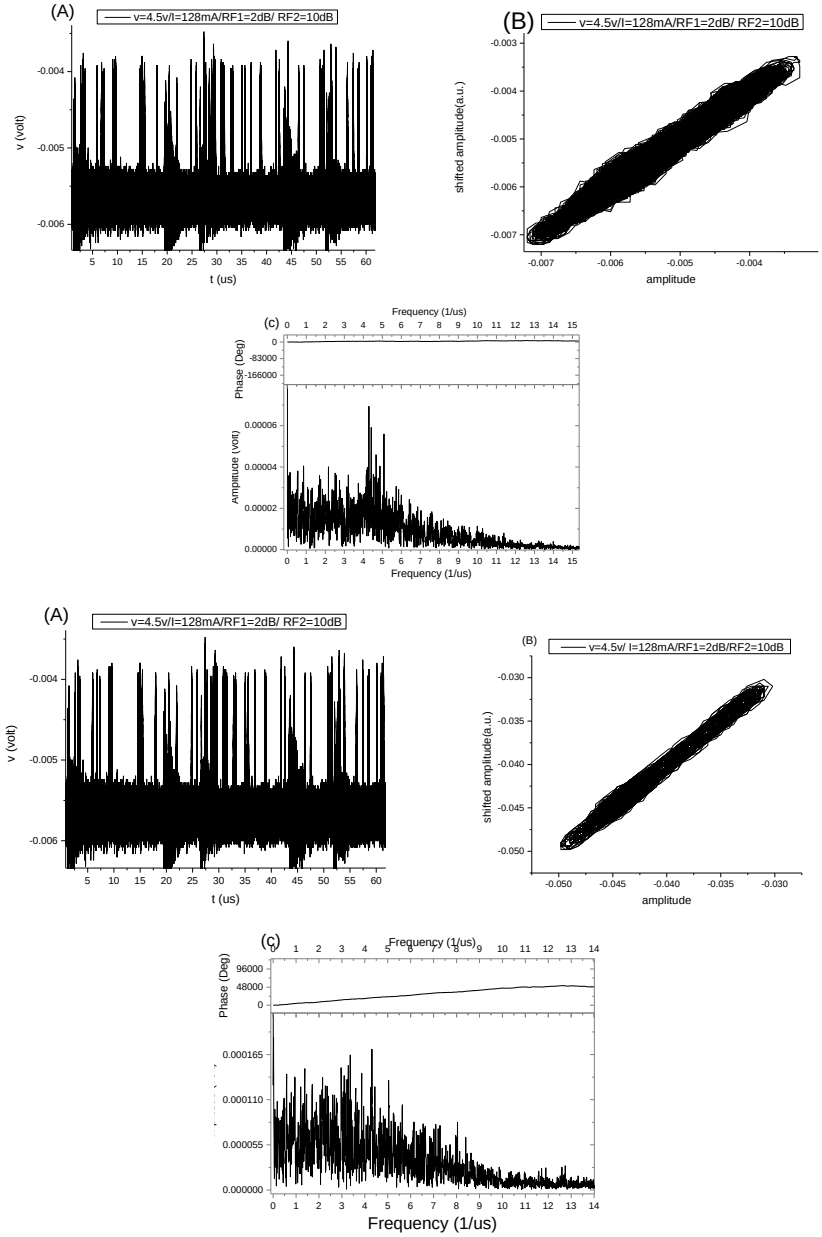

Figure 9 : Results for run no. (5) given in Table (1**).** (A) Time of series, (B) Calibrated attractor, and (C) F.F.T.

The feedback strength was reduced for the same last bias voltage taken in run no. 5 shown in Figure 9, as shown in Figure 10. The resulting dynamics responded directly to signal pulsation in several modes. These modes can be seen in the frequency domain with a broadened Gaussian spectrum. Such dynamics agrees with that reported by Ohtsubo [27].

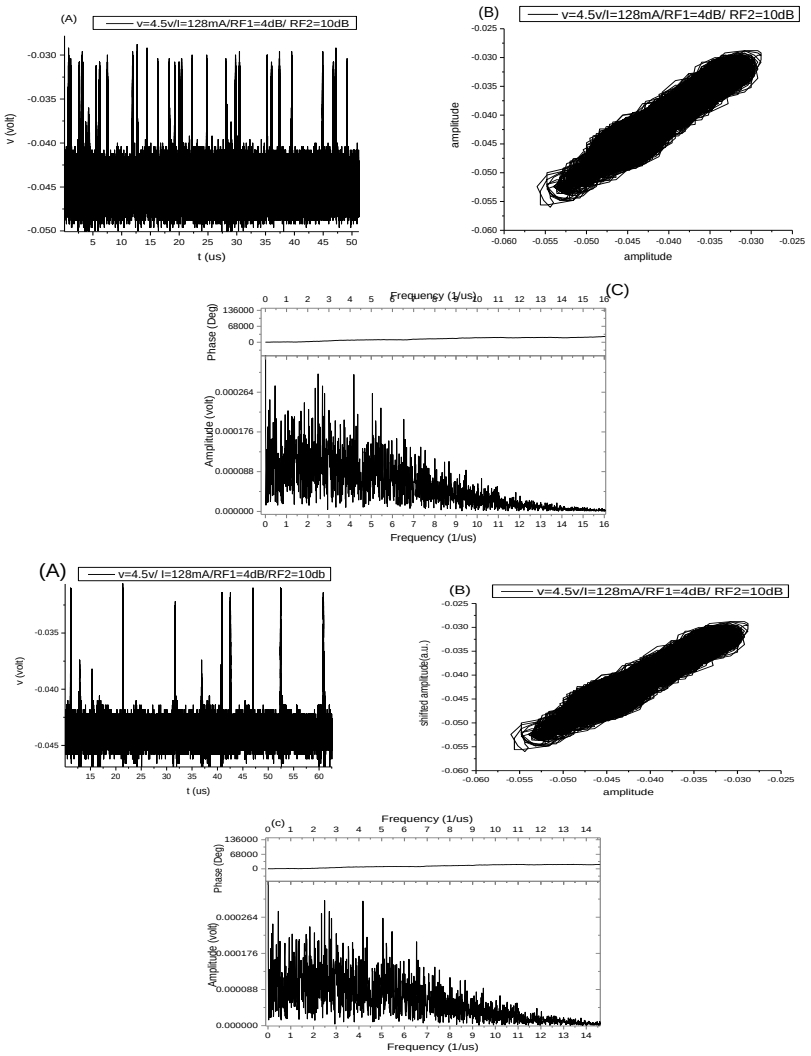

Figure 10 : Experimental results for run no.6 given in Table1 (1). (A) Time series, (B) Calibrated attractor, and (C) F.F.T.

An increase in the difference between the two signal branches led to more noticeable variations between the two observed time series, as shown in Figure (11) compared with the results given by Madhloom et al. [28].

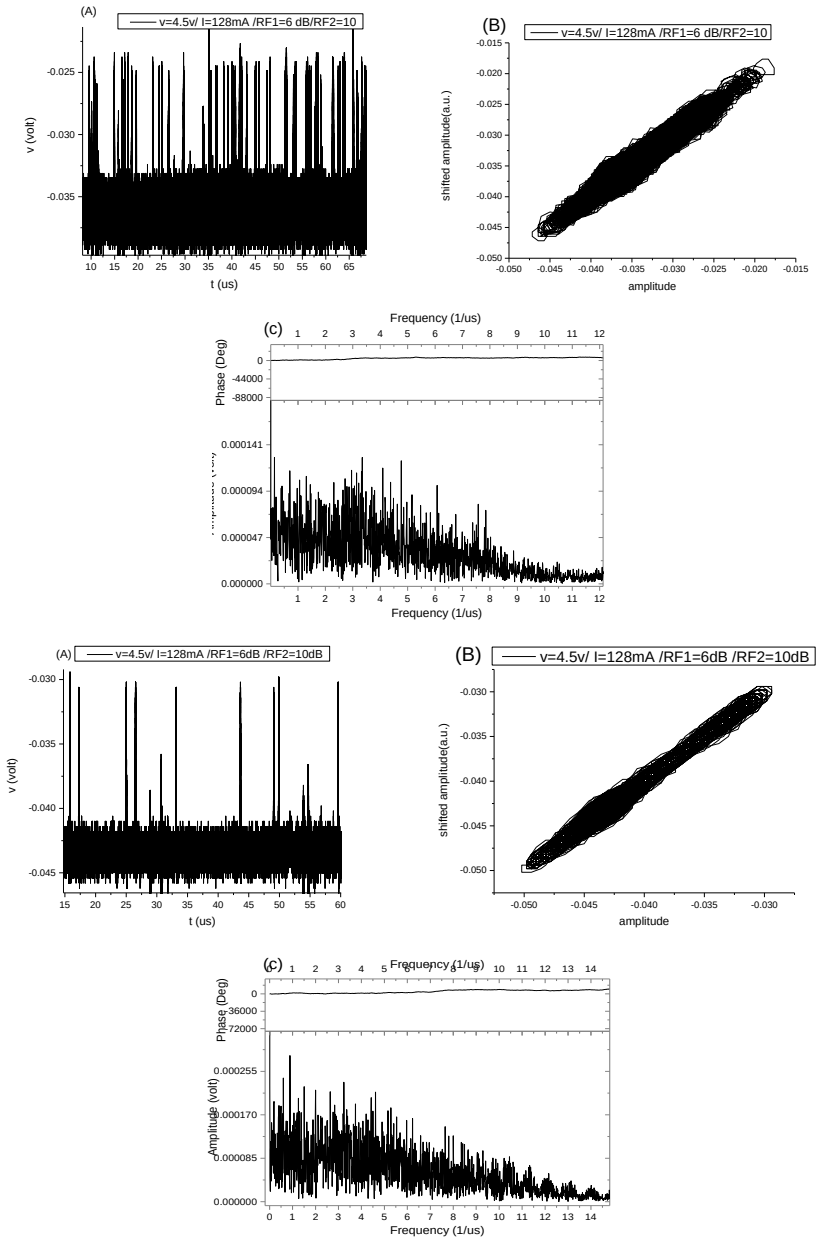

Figure 11: Results for run no. 6 and parameters given in Table (1). **(**A) Time of series, (B) Calibrated attractor, and (C) F.F.T.

Although the amplitudes decreased, the two signal branches remained observable. Variation between them still exist. Meanwhile, any small difference in one applied parameter for this configuration gives rise to summed dynamics. The signal-to-noise ratio was high enough to ensure signal amplitudes, and the noise level in one branch was higher than in the other due to the expected disturbance in the detectors, PD1 and PD2, and the amplifier noise power. The last factor is affecting last ratio via the denominator.

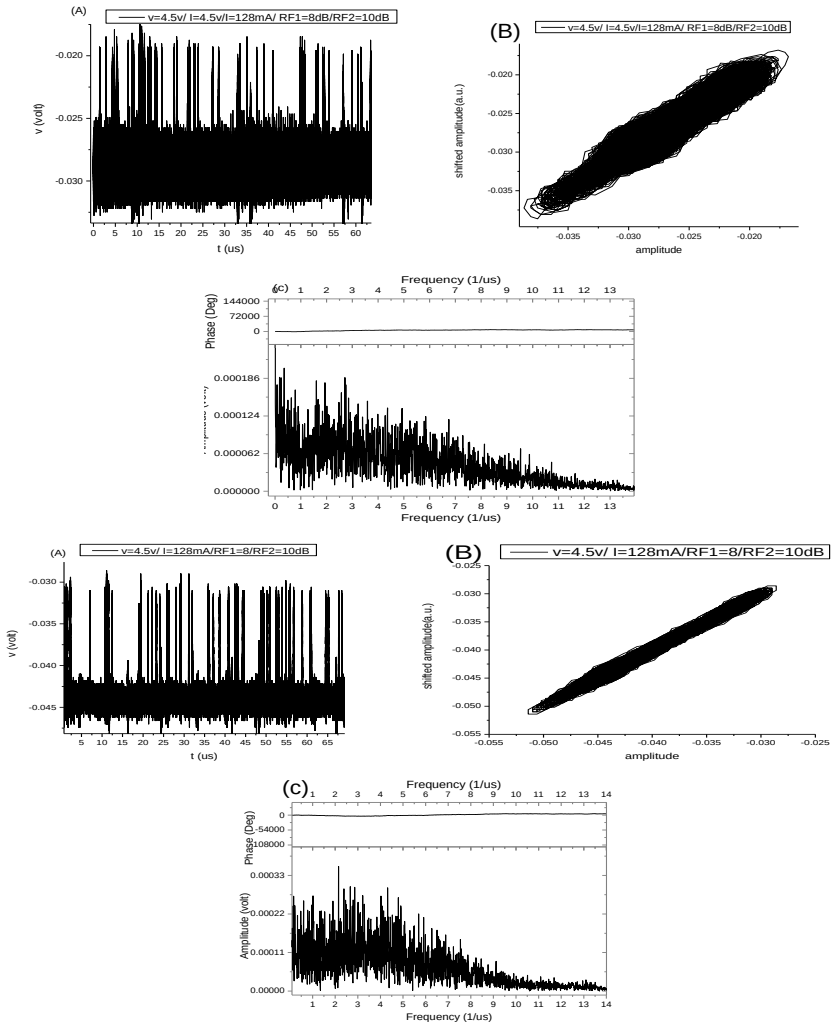

Figure 12: Experimental results for run no.7 listed in Table (1). (A) the Time series, (B) Calibrated attractor, and (C) FFT.

5. Conclusions

To achieve two different signal weights from one SL device with enriched dynamics signals, it is effective, primarily, to demultiplex and filter the SL optical power into two parts. De-multiplexing can offer many feedback levels that permit fine selection for perturbation to re-inject them back into the ISL bias as a chaotic modulation. Variation in each signal gives rise to overall dynamics. This allows interplaying signal weights by changing one or more of its parameters. Increase of filtering using a narrower filter led to power reduction. This translates SL active medium into new quantum emission states within bifurcation diagram. This variety of emissions is located in the directory of chaotic dynamics, which is the main requirement for introducing coding for sent signals. The feedback itself can play another important role, which is the learning term in an optical neural network. The calibration between electrochemical and optical signals is a promising technique to develop the field of SL optically.

Acknowledgments. Authors would like to thank both of Al-Nahrain University for the support and Mustansiriyah University for the cooperation.

References

[1] W. S. McCulloch and W. Pitts, "A logical calculus of the ideas immanent in nervous activity," *Bull. Math. Biophys*, vol. 5, no. 4, pp. 115-133, 1943.

[2] R. F. Thompson, "The neurobiology of learning and memory," *Science*, vol. 233, no. 4767, pp. 941-947, 1986.

[3] A. L. Hodgkin and A. F. Huxley, "Quantitative description of membrane current and its application to conduction and excitation in nerve," *The Journal of Physiology*, vol. 117, pp. 500-544, 1952.

[4] E. M. Izhikevich, "Dynamical Systems in Neuroscience: The Geometry of Excitability and Bursting," London, England: The MIT Press-Cambridge, Massachusetts, 2007.

[5] S. Pasricha and M. Nikdast, "A Survey of Silicon Photonics for Energy-Efficient Manycore Computing," *IEEE Design & Test*, vol. 37, no. 4, pp. 60-81, 2020.

[6] F. P. Sunny, E. Taheri, M. Nikdast and S. Pasricha, "A Survey on Silicon Photonics for Deep Learning," *ACM Journal on Emerging Technologies in Computing Systems*, vol. 17, no. 4, pp. 1-57, 2021.

[7] J. W. Goodman, A. R. Dias, and L. M. Woody, "Fully parallel, high-speed incoherent optical method for performing discrete Fourier transforms," *Optics Letters***,** vol. 2, no. 1, pp. 1-3, (1978).

[8] X. Hu, A. Wang, M. Zeng, Y. Long, L. Zhu, L. Fu and J. Wang, "Graphene-assisted multiple-input high-base optical computing," *Scientific Reports*, vol. 6, p. 32911, 2016.

[9] T. L. Szabo, "Diagnostic Ultrasound Imaging: Inside Out," Second Edition, Boston, MA, USA: Academic Press, 2014.

[10] G. P. Agrawal, "Nonlinear effects in optical fibers," Institute of Optics University of Rochester, Rochester, NY, 2006.

[11] A. A. Hemed, M. M. Fdhala and S. M. Khorsheed, "Modified superstructure fiber Bragg grating for a filter application," *Kuwait Journal of Science*, vol. 49, no. 1, pp. 1-18, 2022.

[12] A. F. G. F. Filho and J. S. Chaves, "Sensors of encoding and decoding based on superstructures fiber Bragg gratings modulated in amplitude and phase for applications in systems OCDMA-63 chip," *Fiber and Integrated Optics*, vol. 38, no. 6, pp. 349-361, 2019.

[13] D. Zhang and D. Zhang, "A Review of Optical Neural Networks," *Appl. Sci.*, vol. 12, no. 11:5338, pp. 1-14, 2022.

[14] I. Goodfellow, Y. Bengio and A. Courville, "Deep Learning," The MIT Press, Cambridge, MA, USA, 2016.

[15] N. P. Jouppi, C. Young, N. Patil, N. Patil, G. Agrawal, R. Bajwa and et.al., "In-Datacenter Performance Analysis of a Tensor Processing Unit," in *Proceedings of the 44th Annual International Symposium on Computer Architecture*, Toronto ON Canada, 2017.

[16] S. Dhar, D. Pan, R. Soref, R. Z. Chen, Z. Wang and Z. Zhao, " Silicon microdisk-based full adders for optical computing," *Opt. Lett.*, vol. 43, pp. 983-986, 2018.

[17] A. H. Al-Hamdani, H. G, Rashid and Z. R. Ghayib, "Improvement of laser to fiber coupling efficiency using microlens technique," *ARPN J. of Eng. and App. Sci.*, vol. 9, no. 11, pp. 2286-2291, 2014.

[18] A. A. Hemed, Z. R. Ghayib and H. G. Rashid, "Controlling a chaotic anti-synchronized oscillator by a phase interplayed optical injected seed with an FBG sensor," *J. Phys.: Conf. Ser.*, vol. 1963, p. 012063, 2021.

[19] J. S. Suelze, Double optical feedback and PT-symmetry breaking induced nonlinear dynamics in semiconductor lasers, West Lafayette, Indiana: Purdue University, 2016.

[20] E. Mercier, High-frequency nonlinear dynamics of a laser diode with phase-conjugate feedback, France: LMOPS: Autre. CentraleSupélec, 2016.

[21] H. Erzgraber, B. Krauskopf, and D. Lenstra, "Bifurcation Analysis of a semiconductor laser with Filtered Optical Feedback," *SIAM J. Applied dynamics systems*, vol. 6, no. 1, pp. 1-28, 2007.

[22] Z. R. Ghayib and A. A. Hemed, "Smart control for the chaotic dynamics using two regions uniform fiber Bragg grating," *Optoelectronics and advanced materials-Rapid communications*, vol. 16, no. 7-8 July-August, pp. 307-318, 2022.

[23] A. A. Hemed and H. A. Abbas, "Experimental diagnose for spikes width relation with positive optoelectronic feedback attenuation in a quantum well laser diode," *AIP Conf. Proc.*, vol. 2834, no. 1, p. 070001, 2023.

[24] M. Dhyaa, A. Hemed and H. Rasheed, "Effect of phase shifted signal propagated in optical fiber into minor laser neural network," *AIP Conf. Proc.*, vol. 3036, no. 1, p. 050020, 2024.

[25] A. A. Hemed and Z. R. Ghayib, "Effect of Partial Optically Filtered Optoelectronic Feedback on Laser Diode Chaotic Emission," in *2022 4th International Conference on Current Research in Engineering and Science Applications (ICCRESA)*, Baghdad, Iraq, 2022, pp. 165-171, doi: 10.1109/ICCRESA57091.2022.10352449., 2023.

[26] F. Rosenblatt, "The Perceptron — A Perceiving and Recognizing Automaton," UMass Amherst, Massachusetts, 1957.

[27] J. Ohtsubo, "Dynamics of Semiconductor Lasers with Optoelectronic Feedback and Modulation," in *Semiconductor Lasers*, vol. 111, Berlin, Heidelberg, Springer Series in Optical Sciences, vol. 111. Springer, 2008.

[28] D. R. Madhloom, A. A. Hemed and S. M. Khorsheed, "Experimental Simulation for Two Optically Filtered Modulation Weights in Laser Diode as a Self-Learning Layer," *East European Journal of Physics*, no. 2, pp. 267-276, 2023.